Machine Learning Magnetism Classifiers from Atomic Coordinates

Helena A Merker[1,2,*], Harry Heiberger[1,2,*], Linh Nguyen[1,3,*], Tongtong Liu[1,3,*], Zhantao Chen[1,4], Nina Andrejevic[1,5], Nathan C. Drucker[1,6], Ryotaro Okabe[1,7], Yao Wang[8], Tess Smidt[2,†], and Mingda Li[1,9,†]

[1] *Quantum Measurement Group, Massachusetts Institute of Technology, Cambridge, MA 02139, USA*
[2] *Department of Electrical Engineering and Computer Science, Massachusetts Institute of Technology, Cambridge, MA 02139, USA*
[3] *Department of Physics, Massachusetts Institute of Technology, Cambridge, MA 02139, USA*
[4] *Department of Mechanical Engineering, Massachusetts Institute of Technology, Cambridge, MA 02139, USA*
[5] *Department of Materials Science and Engineering, Massachusetts Institute of Technology, Cambridge, MA 02139, USA*
[6] *Department of Applied Physics, Harvard University, Cambridge, MA 02138, USA*
[7] *Department of Chemistry, Massachusetts Institute of Technology, Cambridge, MA 02139, USA*
[8] *Department of Physics, Clemson University, Clemson, SC 29634, USA*
[9] *Department of Nuclear Science and Engineering, Massachusetts Institute of Technology, Cambridge, MA 02139, USA*
[*] *Equal first authors*
[†] *Corresponding authors: mingda@mit.edu, tsmidt@mit.edu*

Abstract

The determination of magnetic structure poses a long-standing challenge in condensed matter physics and materials science. Experimental techniques such as neutron diffraction are resource-limited and require complex structure refinement protocols, while computational approaches such as first-principles density functional theory (DFT) needs additional semi-empirical correction, and reliable prediction is still largely limited to collinear magnetism. In this work, we present a machine-learning model that aims to classify the magnetic structure by inputting atomic coordinates that contain transition metal and rare-earth elements. By building an equivariant Euclidean neural network that preserves the crystallographic symmetry, the magnetic structure (ferromagnetic, anti-ferromagnetic, and non-magnetic) and magnetic propagation vector (zero or non-zero) can be predicted with an average accuracy 77.8% and 73.6%, respectively. In particular, a 91% accuracy is reached when predicting no magnetic ordering even it contains magnetic element(s). Our work represents one step forward to solve the grand challenge of full magnetic structure determination.

1 Introduction

As one of the most prominent quantum phenomena, magnetism of materials encompasses a large portion of functional applications such as data storage [1], high-resolution imaging [2], spintronic devices [3], high-energy scientific instruments [4, 5], and quantum computing [6, 7]. Particular types of magnetism are also believed to be associated with unconventional quantum phases such as high-T_c and topological superconductivity [8]. Unlike small molecules where magnetic structures contain only several high-spin and low-spin configurations, spatial correlations between magnetic moments in sizeable materials constitute vast possibilities of different magnetic configurations. With infinite combinations of wavevectors, moments, and correlations lengths, magnetic materials can form a variety of structures such as antiferromagnetism [9], non-collinear magnetism, skyrmions [10], spin glass [11], and quantum spin liquids [12, 13]. Therefore, the determination of magnetic structures, either experimentally or theoretically, is crucial for materials discovery and technological progress in general.

Experimentally, the state-of-the-art neutron scattering [14] and more recently resonant X-ray scattering [15] have enabled the characterization of magnetic structures with atomic-scale resolution. However, these measurements require large-scale neutron sources or synchrotron X-ray radiation and are highly limited by the capacity and beamtime availability. According to the most comprehensive database, only $\sim 1,500$ materials' magnetic structures have been identified through these experimental spectra since the 1950s [16, 17]. Therefore, without order-of-magnitude improvements of these facilities' capacity, a pure experimental exploration of magnetic materials is yet to catch up with the rapidly rising demand for materials' discovery of new magnetic materials.

Theoretically, *ab initio* simulations with advanced quantum chemistry and physics methods have been successfully applied to the prediction of magnetism of small molecules [18]. However, the computational complexity of these accurate methods increases exponentially with the system size, which makes it impractical to be extended to sizeable materials beyond nanoscale. The first-principles DFT simulations and the associated corrections provide an efficient compromise between accuracy and scalability. Although the delocalization error and the lack of static correlation may underestimate the magnetic moment and correlations [19, 20], DFT-based methods have enabled high-throughput calculations over ∼10,000 materials [21], allowing for preliminary statistical predictions of materials' properties. Even with substantial acceleration compared to experiments and wavefunction-based methods, the computational complexity of DFT calculations is still non-negligible and hinders the discovery in a huge, possibly infinitely large, parameter space of chemical compositions. Moreover, since electronic structure theory evaluates the energy for a specific electronic configuration, including the magnetic structure, the standard simulation requires traversing all configurations for a single atomic structure and determining the ground-state magnetic configuration. Thus the large number of possible magnetic configuration forms a "guessing-computing" duo; that is, guessing many possible configurations and computing them one by one. Consequently, most computational efforts are spent on irrelevant magnetic excited states rather than the true ground states. A reliable prediction of the ground-state magnetic structure would greatly accelerate high-throughput calculation and bring us closer to achieving simulation-free materials discovery.

Given the challenges in magnetic structure determination from experiments and calculations, significant research effort has recently been dedicated to using machine learning to enhance magnetic structure determination. Some recent works combine DFT calculations with machine learning [22–25], in some of which the "guessing" step in the guessing-calculating procedure is obtained with machine learned models. For instance, machine learning has been implemented to reduce the search space of possible magnetic configurations in the "guessing" step. With this approach, the main calculation task is still carried out by the standard first-principles DFT calculations. Some other works are based on model Hamiltonians [26, 27], mostly classical spin models, and use machine learning methods to fit the free parameters in such a model, such as from experimental data that contain the spin information. Even so, the direct prediction of magnetic structure from the more direct atomic structure, aka replacing the "computing" step, is still challenging.

A full description of magnetism[28] can be nontrivial. In this work, we focus on two different descriptions that use relatively few variables: magnetic order labels and propogation vectors. Magnetic ordering labels (e.g. ferromagnetic (FM) and antiferromagnetic (AFM)) are helpful because they summarizes the complexity of magnetic structures into simple classes that are application relevant. A propagation vector is a vector in reciprocal space that describes symmetry breaking due to the presence of a magnetic order. A non-zero propagation vector is one indicator for a more involved magnetic structure beyond the FM, AFM and NM ternary classification. While these description are expressive, they are not comprehensive and we leave more complex descriptions of magnetic order to future work.

We build an ML-based classifier that predicts the magnetic order under a ternary classification (FM/FiM: ferromagnetic/ferrimagnetic, AFM: antiferromagnetic, NM: non-magnetic), and also outputs whether the propagation vector is zero or non-zero. We choose these two in our prediction as a start, in doing so, we acquire partial but valuable information that may accelerate full magnetic structure determination. Our work differs from some prior efforts in that, after training, the predictive model can directly output the magnetic order and propagation vector with only atomic structure as the input, without requiring any further first-principles calculations. This is realized by applying the Euclidean neural network (E(3)NN), which preserves 3D rotation, inversion and translation symmetry in the atomic structures, so that high accuracy is reached without data augmentation [29]. The accuracy in test set is about 78% for magnetic order prediction and about 74% for propagation vector prediction. The accuracy varies when the material of interest contains different elements or belongs to different space groups, as we will elaborate in the results section. Since the magnetic order and propagation vector represent two different pieces of magnetic structure information, they are trained separately with different neural network architectures and training data from the Materials Project and MAGNDATA [16, 17] databases, respectively. The atomic structure inputs for magnetic order classifiers are from Materials Project, magnetic order labels are obtained using pymatgen's magnetism analyzer given structures with atoms decorated with DFT calculated magnetic moments as inputs. Both structures and propagation vectors for propagation vector classifiers are from MAGNDATA.

2 Methodology

2.1 Data assembly

In order to train the magnetism classifier, we assemble a dataset containing both structure and magnetic order information from the Materials Project [21]. We query structures that contain at least one magnetic elements, including transition metals (Sc, Ti, V, Cr, Mn, Fe, Co, Ni, Cu, Y, Nb, Mo, Ru, Rh, Re, Os, Ir, Pt), lanthanides (Ce, Pr, Nd, Sm, Eu, Gd, Tb, Dy, Ho, Er, Tm, Yb), and/or actinides (Th, U, Np, Pu); however, a material containing a magnetic element does not necessarily host magnetic order. Our search is restricted to calculations using the generalized gradient approximation with Hubbard interaction (GGA+U), which is suitable for magnetic structure calculations and leads to a total of 34,856 structures[1], among which 30,584 are FiM/FM, 1,790 are AFM and 2,482 are NM. The magnetic order labels are derived using the Python-based pymatgen analysis code [30] and through use of a CollinearMagneticStructureAnalyzer class. The CollinearMagneticStructureAnalyzer class uses the DFT calculated magnetic moments and total magnetization (the absolute value of the sum of individual magnetic moments) to assign one of the following labels: FM if the total magnetization is greater than zero and all magnetic moments have the same sign, FiM if the total magnetization is greater than zero, AFM if total magnetic moment is zero and max absolute magnetic moment greater than zero, or NM magnetic order if total and max magnetic moment is zero. We then train 20 classifiers with different initial weights, each optimized on a randomly selected subset of 6,086 structures with a AFM:FM:NM ratio of 5:6:6. The size of each class is kept comparable in each selected subset to mitigate the training bias toward nonmagnetic examples, since there is a substantially larger fraction of FM/FiM structures in the total dataset and only 1,790 AFM examples. Each subset of 6,086 materials is divided among training, validation, and test sets with a ratio of 0.8:0.1:0.1. Note that we find this further improves our model's ability to differentiate between AFM and FM/FiM classes, and the smaller data size helps reduce the overall training time.

Magnetic materials may host more complex magnetic structures beyond AFM/FiM which are described by other non-zero magnetic propagation vectors. In order to capture this complexity, we further train a binary classifier of the propagation vector magnitude (zero or non-zero). The zero propagation vector represents the prototypical FM order, while the non-zero propagation vector represents AFM/FiM orders and beyond. We obtain the structure and magnetic propagation vector information from the MAGNDATA database [16, 17], which to date contains the comprehensive experimentally-determined magnetic structures of 1,562 compounds. The data used in this study were restricted to commensurate magnetic structures, as incommensurate magnetic structures always have non-zero propagation vectors. This yielded 1,134 total structures, of which 552 (582) have zero (non-zero) propagation vectors. We again train 20 classifiers with different initial weights, independently dividing the 1,134 total structures at random among training, validation and test sets with a ratio of 0.8:0.1:0.1 for each model. To link the propagation vector classification with that of magnetic order, we show the statistics of structures appearing in the propagation vector classification datasets in Fig. 1. Some structures' magnetic orders are unknown to pymatgen's magnetism analyzer which we use for determining magnetic order, so those are not included in the figure. Most structures with nonzero propagation vector are AFM, some are FiM, and none are FM or NM, as expected. The propagation vector classifier can further divide AFM and FiM classes into sub-classes with zero/nonzero propagation vector, giving us more information about the magnetic structure of a material.

2.2 Model architecture

The architecture of both classifiers is based on Euclidean Neural Networks (E(3)NNs) [29], a class of 3D Euclidean group (E(3))-equivariant neural networks. Any space group that describes the crystal geometric symmetries in three dimensions is a subgroup of E(3), and thus E(3)NNs preserve all geometric symmetries of the crystal structure, which removes the need for extensive data augmentation needed to consider arbitrary translations or rotations of the input structures. The neural network inputs consist of a material's crystal structure and one or more descriptors of each constituent atom. Specifically, the unit cell of each example is first converted into a periodic graph, where each node a represents an atom described by a feature vector x_a. A single convolutional layer operates on the input x_a and the radial distance vectors $\vec{r}_{ab}$ between atoms a and b in the neighborhood of a up to a radial cutoff $r_{\max} = 5$Å, as

[1]Due to recent updates in the Materials Project, if querying in latest pymatgen version with the same magnetic elements, the number of total structures may change. Our models are trained and tested based on pymatgen version 2022.0.8, with 34,856 total structures after querying.

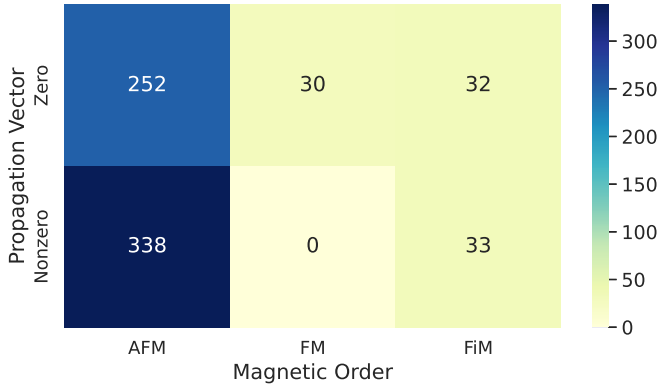

Figure 1: Number of examples with zero and nonzero propagation vector in each magnetic ordering class.

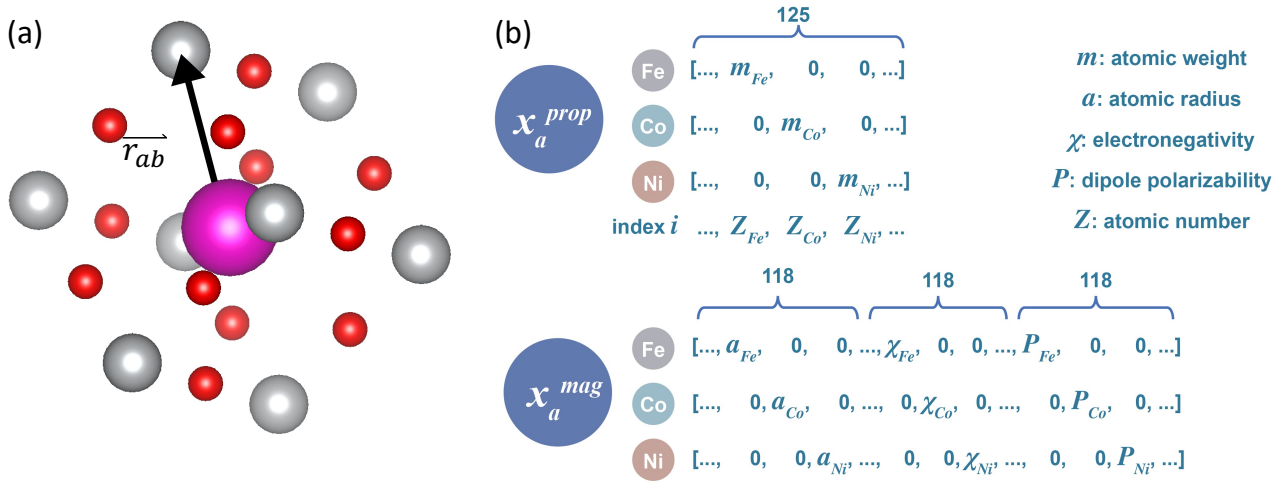

Figure 2: **Illustration of input data structures.** (a) A representative periodic graph constructed from the crystal structure in the neighborhood of a given atom. Each atom (node) carries a feature vector x_a, and each edge connecting node a to a neighboring node b is characterized by the relative distance vector $\vec{r}_{ab}$. (b) Each atom is represented by a node in the periodic graph, and the atom type is expressed by a property-weighted one-hot feature vector. The top row shows a set of representative feature vectors used for the propagation vector classifier. Each is an array of 125 scalars, with the Z-th scalar being the atomic mass in amu (atomic mass unit), where Z denotes the atomic number. The bottom row shows a set of representative feature vectors used for the magnetism classifier. Each is an array of 3×118 scalars, formed by concatenating three arrays of 118 scalars which encode the atomic radius(pm), electronegativity on a Pauling scale, and dipole polarizability(a.u.) of a given atom employing the same property-weighted one-hot encoding scheme used for the propagation vector classifier input.

shown in Fig. 2a. The feature vector x_a associated with each node is constructed by a property-weighted one-hot encoding of selected atomic properties, illustrated in Fig. 2b. For the propagation vector classifier, each feature vector is an array of 125 scalars, with the Z-th scalar being the atomic mass in amu (atomic mass units), where Z denotes the atomic number. Additional properties can be considered by simple concatenation of several such feature vectors, each weighted by the appropriate value of the property of interest. For example, each of the input feature vectors used for the magnetism classifier is an array of 3×118 scalars, formed by concatenating three arrays of 118 scalars that encode the atomic radius (pm), electronegativity on a Pauling scale, and dipole polarizability (a.u.). The architecture of both classifiers consists of three principal parts, as shown in Fig. 3. First, the input feature vectors are passed to an embedding layer for dimensionality reduction. The E(3)NN layers are then applied to the resulting hidden state and consist of alternating convolution and gated block operations (dashed rounded rectangle).

The convolution signifies the tensor product between input feature vectors and symmetry-constrained convolutional kernels. The convolution step is implemented as:

$$f_a' = \frac{1}{\sqrt{z}} \sum_{b;|\vec{r}_{ab}|<r_{max}} f_b \otimes (h(\|\vec{r}_{ab}\|))\, Y(\vec{r}_{ab}/\|\vec{r}_{ab}\|)$$

where the node f_a' is the output node for the atom a. The output node is the sum of the tensor product between the input node of a neighborhood atom f_b and the neural networks h. Y is the spherical harmonics, which serve as basis functions that enable the mapping of the relative distances to the weights of the tensor product. z is the average degree of the nodes, that is the number of atoms surrounding the center atom. The prefactor $1/\sqrt{z}$ adjust the different number of the neighborhoods. The gated block step denotes a gated rotation-equivariant nonlinearity as described in Ref. [31]. The gate activation is a direct sum of two sets of irreducible representations. Mathematically, this can be written as:

$$\left(\bigoplus_i \phi_i(x_i)\right) \oplus \left(\bigoplus_{l,m} \phi_j(g_{lm}) y_j\right)$$

The first set of the irreducible representation is the scalars x_i passing through activation functions ϕ_i. The second set is the gated scalars g_{lm} passing through activation functions ϕ_j and multiplied by the scalars y_j. The number of functions in the list should match the number of irrep groups in irreps gates.

Finally, the E(3)NN output is converted to a class label by first adding together the output vectors for all atoms in a given material, and then applying a final nonlinear activation. For the propagation vector classifier, the output is a sigmoid-activated scalar, while for the magnetism classifier, it is a softmax-activated array of three scalars giving the probability of exhibiting one of three magnetic orders (AFM, FM/FiM, NM).

3 Results and Discussion

To quantify the consistency of predictions made by the magnetism and propagation vector classifiers, we independently train 20 models for each task using randomly drawn data subsets as described in Section 2.1 above. For the magnetic order classification, we show the test set accuracies of the 20 models in the left panel of Fig. 4, which range from 73.8% to 80.7% and have a mean accuracy of 77.8%. For the propagation vector classification, the test accuracies obtained from 20 models are displayed in the right panel, ranging from 68.1% to 85.0% with a mean of 73.6%, the thresholds of this binary classification are chosen separately for each model to guarantee maximal accuracy. In Table 1 and 2, we summarize the averaged precision, recall, and F1-scores over all trained models for the two tasks, respectively. We note that the larger spread of accuracies in propagation vector classification can possibly be attributed to fewer training examples (1,134 total structures taken 907 at a time for training), which are not sufficient for our model to learn all complex connections between crystal structures and propagation vectors. Besides, it may also suggest that the propagation vector contains rich strong correlation effect that cannot be fully characterized by only atomic structures. More details about the performance of both classifiers are apparent in the confusion matrices (CM) shown in Fig. 5. For the magnetic order classifier, we observe excellent separation of the NM class from the two magnetic classes (Fig. 5(a)). Since all calculations are performed at $T = 0$K, we believe that this non-magnetic separation is important in rapidly screening and excluding materials that do not host any magnetism, without having to experimentally cool down to the lowest measurable temperature. More ambiguities appear between classifications of the AFM and FM/FiM classes, where magnetic orders exist in both classes but in different formats. This is possibly due to the difficulty of distinguishing between FiM and AFM from atomic structures, and the energy difference between magnetic structures with AFM and FM/FiM orders can be small. The overall CM suggests good capability of recognizing potential magnetic orders but slightly weaker ability to identify the exact class. Fig. 5(b) depicts the CM for the propagation vector classifier. Although the overall performance is hard to be considered satisfactory, as already mentioned above, the model has the better precision versus the recall for the non-zero propagation vector.

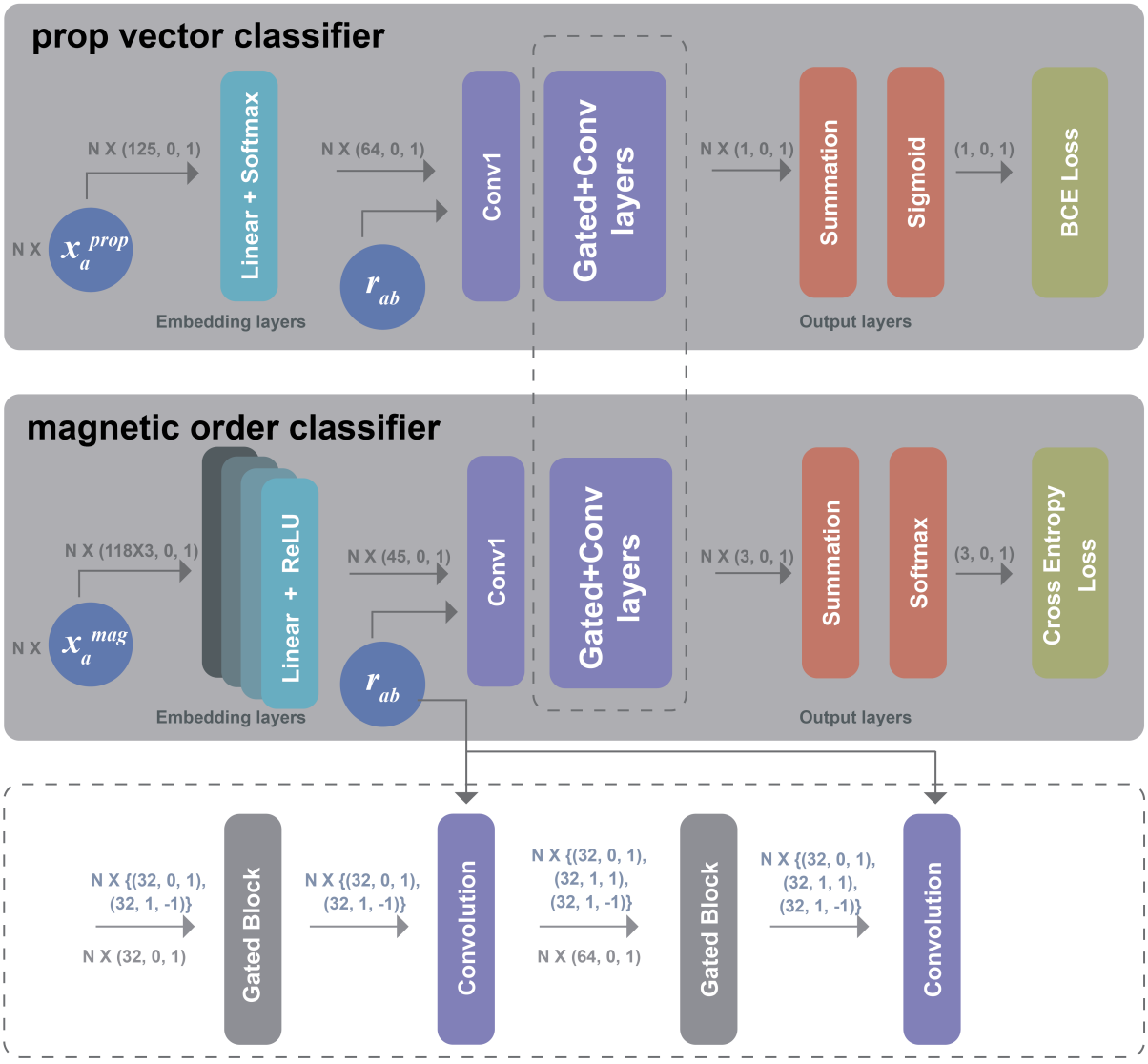

Figure 3: **Illustration of the neural network architectures for propagation vector (top block) and magnetic order classification (middle block)**. The models each consist of three principal layers: embedding layers, convolution and gated layers based on E(3)NN, and the output layers which generate the predicted classes. The convolution and gated layers of both models share the same architecture (detailed architecture shown in the bottom block). Even though the loss functions and embedding layers are optimized separately, by adopting this approach, one atomic structure can lead to a simultaneous prediction of both magnetic order and propagation vector.

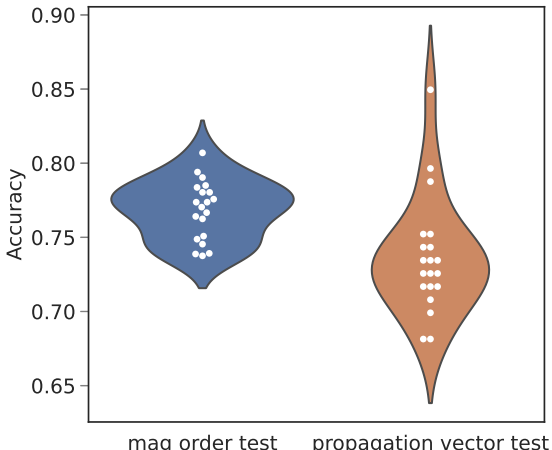

class	precision	recall	f1-score
NM	0.91	0.92	0.91
AFM	0.70	0.68	0.69
FM	0.68	0.70	0.69

Table 1: Averaged metrics of the 20 magnetic order classification models in test sets.

class	precision	recall	f1-score
Zero	0.70	0.83	0.76
Non-zero	0.79	0.64	0.71

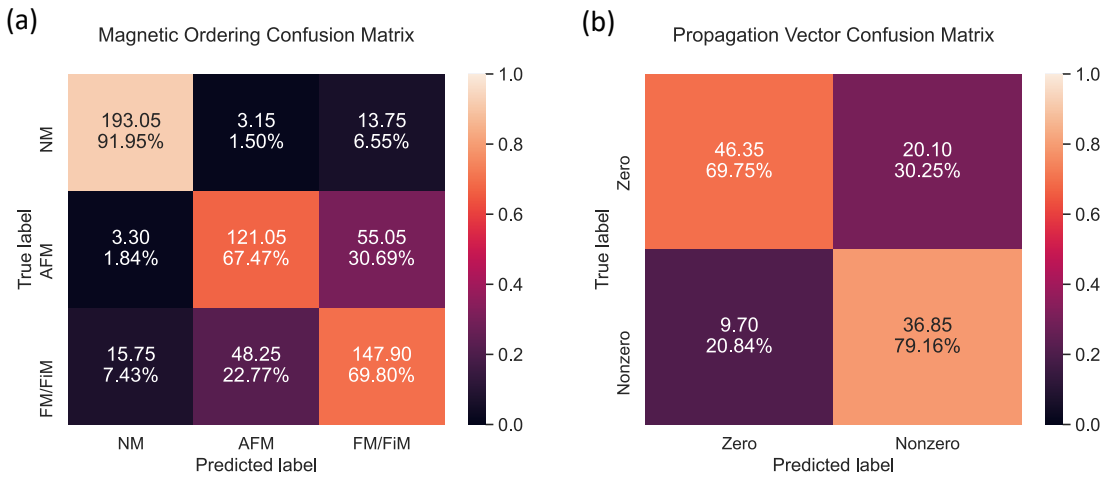

Figure 5: Confusion matrices for prediction results on test sets of (a) magnetic orders and (b) propagation vectors. The values are averaged over 20 models, the color represents the percentage.

To analyze the performance of the magnetism classifier in more detail, we visualize the element-specific test set accuracies in Fig. 6(a). We observe highest classification accuracy on examples containing elements commonly found in ferromagnetic materials, such as Fe, Co, and Ni, with accuracies exceeding 76%. In addition, materials containing certain rare earth elements such as Tb, Dy, and Ho are classified with similar level of accuracy.

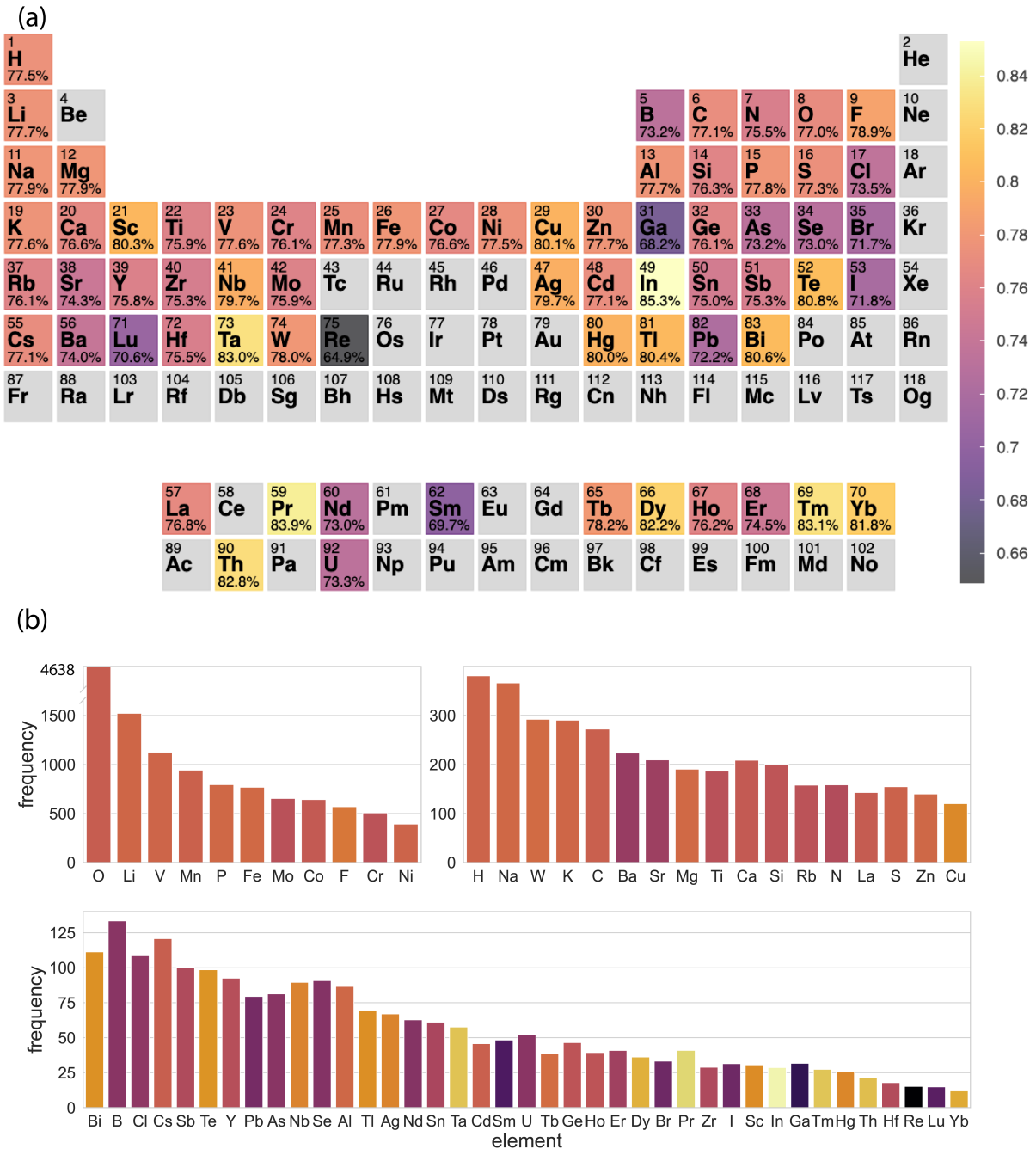

Figure 6: Performance on the testing set and sample statistics of the training set for the magnetic order predictions. (a) The testing accuracy of magnetic order classification per element shown in a color map on a periodic table, grey color indicates the element is absent or insufficient (mean frequency less than 1) in testing sets. (b) Histogram of frequency each element appears in the training sets. The following elements are greyed out due to their absences or insufficiency in test compounds: Pd, Th, Re, Yb, Ce, Eu, Os, Ir, Pt, Rh, Ru, and Np.

To further understand varying accuracies across different elements from the aspect of data abundances, we show the appearance frequency of each element inside the training set in Figs. 6(b). The correlations between high accuracies of some elements and large numbers of training samples containing those elements, including Mn, Fe, Co, Ni and Cu, can be readily found. On the other hand, the elements with lower prediction accuracies are typically less common, such as Ga, Lu, Re, and Sm. However, it is worth highlighting the great performance of some rare earth

elements (e.g. Tb, Dy, and Ho) given the small amount of training samples, this is because they usually coexist with other abundant elements, for example, 65.9% of structures that contain Tb, Dy and Ho also contain elements Mn, Fe, Mo, Co, Ni.

Similar connections between the classification accuracy and the number of training samples can be made for different crystal systems. In Fig. 7(a), we show the number of examples of each magnetic order class as a function of the crystal system of the corresponding structure. Fig. 7(b) indicates that higher appearance frequency in training data in general leads to higher classification accuracy in test data. Such relationships suggest that the predictions made by our model is based on not only the atomic species but also their coordinates and the crystal structure.

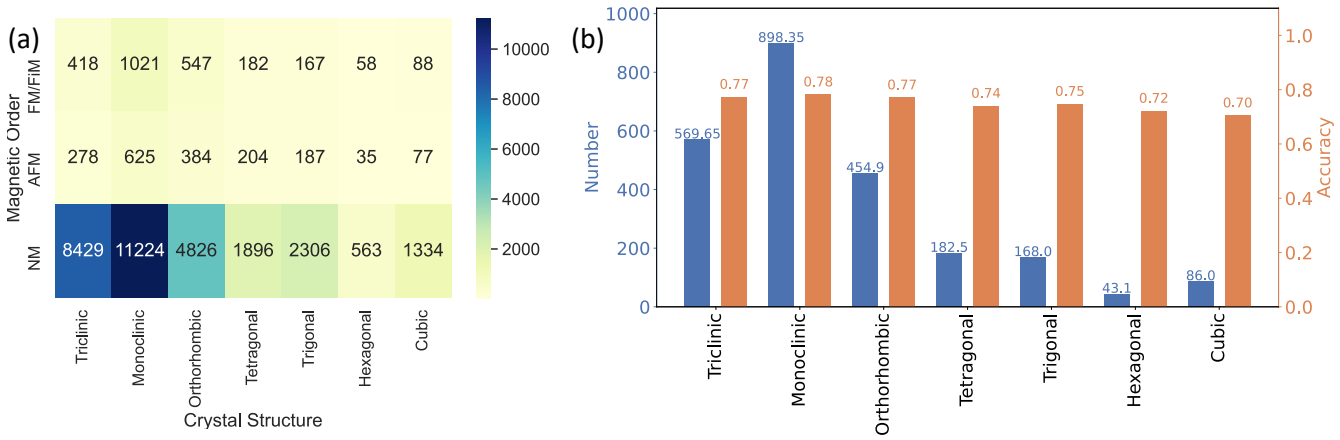

Figure 7: (a) Number of examples in each magnetic order class as a function of the crystal system. (b) Comparison between the number of training samples and testing classification accuracy for each crystal system, the values are averaged over 20 independent models.

4 Discussion

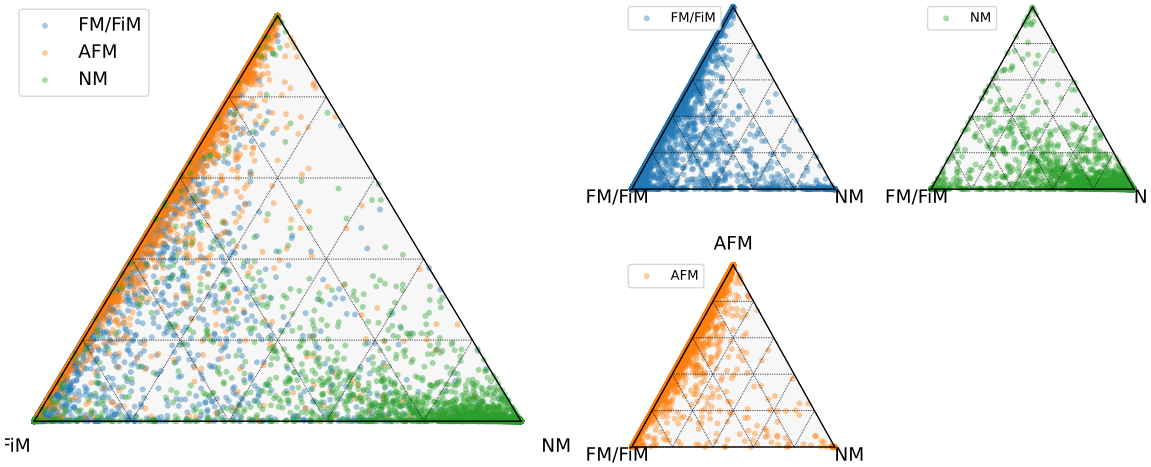

Figure 8: outputs of the neural network with testing data as inputs shown in ternary plots, points represent 3-element vector outputs and are colored by their true label: FM/FiM, AFM and NM.

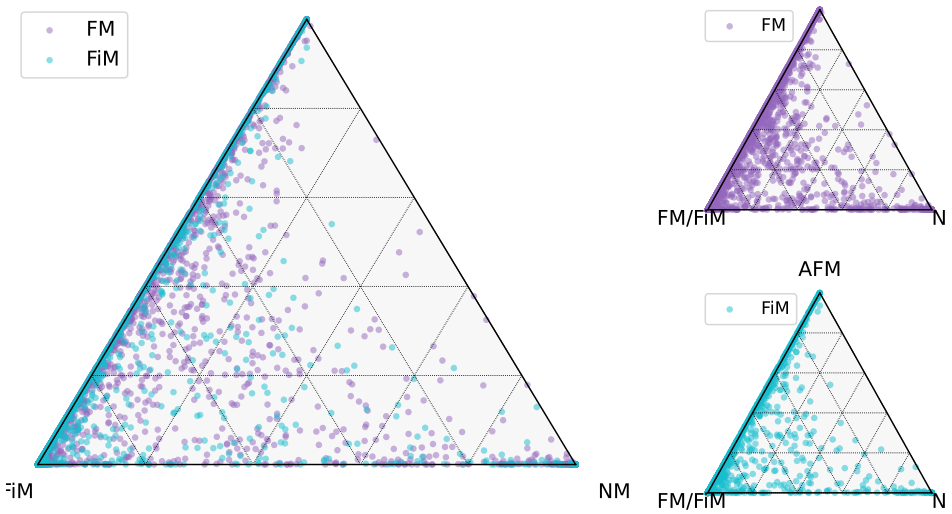

Figure 9: outputs of the neural network with testing data as inputs shown in ternary plots, points represent 3-element vector outputs and are colored by their true label: FM and FiM data.

As mentioned above, our magnetic order classifiers show excellent separation between magnetic (including FM/FiM and AFM) and non-magnetic orders, but more ambiguities between classification of the AFM and FM/FiM classes. To discuss this further, particularly to see whether the FiM is preferably assigned to the FM or AFM class, Fig. 8 and 9 shows the 3-element-vector outputs of the neural network before taking argmax function in a ternary form, with testing data as inputs. The closer a point is to a corner of the triangle, the more likely the predicted label is the corresponding class of that corner. We color the points with their true label to show distinction. Fig. 8 explains that the testing outputs with true labels of AFM and FM/FiM distribute along the edge connecting AFM and FM/FiM classes and do not distinctly separate from each other, which causes the ambiguities in the classification. The data with true label of NM stay close to the NM corner and away from the other two classes. Fig. 9 suggests that our choice to consider FM and FiM order jointly in the class FM/FiM is reasonable, since the distribution of FM and FiM in the ternary plots is similar, and our classifiers treat atomic structures with FM and FiM orders similarly.

In this work, we present a machine-learning based magnetism classifier that takes crystal structure as input and basic magnetic structure information as output. Despite extensive training, it seems that the prediction of magnetism hits a performance barrier, except for the non-magnetic class. This brings up the fundamental query on magnetic representation: besides the atomic species, the interatomic bonding, and the crystal symmetries, there might be some additional information still at large that can capture the essence of magnetism. We anticipate that finding proper magnetic representation can significantly boost the machine-learning on magnetic materials research and shed light on strongly correlated electronic materials in general.

5 Acknowledgments

H.A.M., H.H., and L.N. thank the support from MIT Experiential Learning Opportunities (ELO) Program for first-year students and MIT Undergraduate Research Opportunities Program (UROP) and the Baruch (1947) Fund. T.L. acknowledges the support from MathWorks Science Fellowship. Z.C., N.A. and M.L. acknowledge the support from U.S. DOE, Office of Science (SC), Basic Energy Sciences (BES), award No. DE-SC0021940. M.L. acknowledges the Norman C. Rasmussen Career Development Chair.

6 Declaration of interests

The authors declare no competing interests.

References

[1] A. Fert, "Nobel Lecture: Origin, development, and future of spintronics", Rev. Mod. Phys. **80**, 1517–1530 (2008).

[2] M. T. Vlaardingerbroek and J. A. Boer, *Magnetic Resonance Imaging: Theory and Practice* (Springer Science & Business Media, 2003).

[3] A. Manchon, J. Železný, I. Miron, T. Jungwirth, J. Sinova, A. Thiaville, K. Garello, and P. Gambardella, "Current-induced spin-orbit torques in ferromagnetic and antiferromagnetic systems", Rev. Mod. Phys. **91**, 035004 (2019).

[4] L. Artsimovich, "Tokamak devices", Nucl. Fusion **12**, 215–252 (1972).

[5] H. Wiedemann, *Particle Accelerator Physics* (Springer Nature, Jan. 2015).

[6] N. A. Gershenfeld and I. L. Chuang, "Bulk Spin-Resonance Quantum Computation", Science **275**, 350–356 (1997).

[7] L. Balents, "Spin liquids in frustrated magnets", Nature **464**, 199–208 (2010).

[8] B. Keimer, S. A. Kivelson, M. R. Norman, S. Uchida, and J. Zaanen, "From quantum matter to high-temperature superconductivity in copper oxides", Nature **518**, 179–186 (2015).

[9] C. G. Shull and J. S. Smart, "Detection of Antiferromagnetism by Neutron Diffraction", Phys. Rev. **76**, 1256–1257 (1949).

[10] S. Mühlbauer, B. Binz, F. Jonietz, C. Pfleiderer, A. Rosch, A. Neubauer, R. Georgii, and P. Böni, "Skyrmion Lattice in a Chiral Magnet", Science **323**, 915–919 (2009).

[11] K. Binder and A. P. Young, "Spin glasses: Experimental facts, theoretical concepts, and open questions", Rev. Mod. Phys. **58**, 801–976 (1986).

[12] A. Banerjee, J. Yan, J. Knolle, C. A. Bridges, M. B. Stone, M. D. Lumsden, D. G. Mandrus, D. A. Tennant, R. Moessner, and S. E. Nagler, "Neutron scattering in the proximate quantum spin liquid alpha-$RuCl_3$", Science **356**, 1055–1059 (2017).

[13] Y. Zhou, K. Kanoda, and T.-K. Ng, "Quantum spin liquid states", Rev. Mod. Phys. **89**, 025003 (2017).

[14] S. W. Lovesey, *Theory of Neutron Scattering from Condensed Matter: Volume I: Nuclear Scattering*, International Series of Monographs on Physics (Oxford University Press, Oxford, New York, Oct. 1986).

[15] L. J. P. Ament, M. van Veenendaal, T. P. Devereaux, J. P. Hill, and J. van den Brink, "Resonant inelastic x-ray scattering studies of elementary excitations", Rev. Mod. Phys. **83**, 705–767 (2011).

[16] S. V. Gallego, J. M. Perez-Mato, L. Elcoro, E. S. Tasci, R. M. Hanson, K. Momma, M. I. Aroyo, and G. Madariaga, "*MAGNDATA*: towards a database of magnetic structures. I. The commensurate case", J. Appl. Crystallogr. **49**, 1750–1776 (2016).

[17] S. V. Gallego, J. M. Perez-Mato, L. Elcoro, E. S. Tasci, R. M. Hanson, M. I. Aroyo, and G. Madariaga, "*MAGNDATA*: towards a database of magnetic structures. II. The incommensurate case", J. Appl. Crystallogr. **49**, 1941–1956 (2016).

[18] Z. Li, S. Guo, Q. Sun, and G. K.-L. Chan, "Electronic landscape of the P-cluster of nitrogenase as revealed through many-electron quantum wavefunction simulations", Nat. Chem. **11**, 1026–1033 (2019).

[19] W. Huang, D.-H. Xing, J.-B. Lu, B. Long, W. H. E. Schwarz, and J. Li, "How Much Can Density Functional Approximations (DFA) Fail? The Extreme Case of the FeO4 Species", J. Chem. Theory Comput. **12**, 1525–1533 (2016).

[20] F. Liu, T. Yang, J. Yang, E. Xu, A. Bajaj, and H. J. Kulik, "Bridging the Homogeneous-Heterogeneous Divide: Modeling Spin for Reactivity in Single Atom Catalysis", Front. Chem. **7**, 219 (2019).

[21] A. Jain, S. P. Ong, G. Hautier, W. Chen, W. D. Richards, S. Dacek, S. Cholia, D. Gunter, D. Skinner, G. Ceder, and K. A. Persson, "Commentary: The Materials Project: A materials genome approach to accelerating materials innovation", APL Mater. **1**, 011002 (2013).

[22] T. D. Rhone, W. Chen, S. Desai, S. B. Torrisi, D. T. Larson, A. Yacoby, and E. Kaxiras, "Data-driven studies of magnetic two-dimensional materials", Sci. Rep. **10**, 15795 (2020).

[23] F. Zheng and P. Zhang, "MagGene: A genetic evolution program for magnetic structure prediction", Comput. Phys. Commun. **259**, 107659 (2021).

[24] G. Katsikas, C. Sarafidis, and J. Kioseoglou, "Machine Learning in Magnetic Materials", Phys. Status Solidi B **258**, 2000600 (2021).

[25] N. C. Frey, M. K. Horton, J. M. Munro, S. M. Griffin, K. A. Persson, and V. B. Shenoy, "High-throughput search for magnetic and topological order in transition metal oxides", en, Sci. Adv. **6**, eabd1076 (2020).

[26] D. Wang, S. Wei, A. Yuan, F. Tian, K. Cao, Q. Zhao, Y. Zhang, C. Zhou, X. Song, D. Xue, and S. Yang, "Machine Learning Magnetic Parameters from Spin Configurations", Adv. Sci. **7**, 2000566 (2020).

[27] A. M. Samarakoon, K. Barros, Y. W. Li, M. Eisenbach, Q. Zhang, F. Ye, V. Sharma, Z. L. Dun, H. Zhou, S. A. Grigera, C. D. Batista, and D. A. Tennant, "Machine-learning-assisted insight into spin ice $Dy_2Ti_2O_7$", Nat. Commun. **11**, 892 (2020).

[28] J. Rodríguez-Carvajal and J. Villain, "Magnetic structures", C. R. Phys **20**, 770–802 (2019).

[29] M. Geiger, T. Smidt, A. M., B. K. Miller, W. Boomsma, B. Dice, K. Lapchevskyi, M. Weiler, M. Tyszkiewicz, S. Batzner, M. Uhrin, J. Frellsen, N. Jung, S. Sanborn, J. Rackers, and M. Bailey, *E3nn/e3nn: 2021-08-27*, version 0.3.5, Aug. 2021.

[30] S. P. Ong, W. D. Richards, A. Jain, G. Hautier, M. Kocher, S. Cholia, D. Gunter, V. L. Chevrier, K. A. Persson, and G. Ceder, "Python Materials Genomics (pymatgen): A robust, open-source python library for materials analysis", Comput. Mater. Sci. **68**, 314–319 (2013).

[31] Z. Chen, N. Andrejevic, T. Smidt, Z. Ding, Q. Xu, Y. Chi, Q. T. Nguyen, A. Alatas, J. Kong, and M. Li, "Direct Prediction of Phonon Density of States With Euclidean Neural Networks", Adv. Sci. **8**, 2004214 (2021).